Radiative decay from doubly and singly excited states of He-like nickel

L. Natarajan[1,2] and Riddhi Kadrekar[1]

[1]*Department of Physics, University of Mumbai, Mumbai-400098, India*
[2]*Centre for Excellence in Basic Sciences, University of Mumbai, Mumbai-400098, India*
(Received 21 January 2013; published 2 July 2013)

Fully relativistic calculations on the level energies and radiative lifetimes for all the low-lying levels of He-like Ni have been systematically carried out and attention has been paid to provide a complete tabulation of data for all the conceivable one- and two-electron one-photon transitions from levels of $2p^2$ configuration decaying sequentially to the $^1S_0$ ground state. Large-scale multiconfiguration Dirac-Fock wave functions have been applied to study the level features. The accuracy of our computed data has been highlighted in terms of the uncertainty estimates on the fine structure energy levels and also on the line strengths. The branching ratios of the emitted radiations from various transitions are evaluated. The sensitivity of transition rates to Breit interaction and quantum elctrodynamics effects are analyzed in detail. A comparison of our results with available experimental and previous computations is also made.

PACS number(s): 31.30.Gs

I. INTRODUCTION

Nickel is one of the most cosmically abundant heaviest elements and has been detected in a number of astrophysical bodies [1–7]. The Ni K lines have diagnostic potential in x-ray astronomy in estimating quantities such as red shift, temperature, abundance, and the velocity of emitting gas [8]. The 8-keV x-ray spectra of the K_β satellites from Fe and K_α satellites from Ni overlap each other as these elements are simultaneously present in large tokamaks like Tokamak Fusion Test Reactor (TFTR) and Tore Supra TITR and the information on Fe-Ni line features are important in understanding the properties of the hottest parts of thermal plasmas [9]. Even the low intense electric dipole forbidden $M1$, $E2$, etc., lines in He-like ions play a vital role in understanding the density fluctuations and elementary processes in both astrophysical and laboratory plasmas [10]. Very recently, the production of doubly excited $2p^2$ ($^1D_2$) state in He-like Ar using resonant coherent excitation has been reported by Nakona *et al.* [11]. On the theoretical side, the radiative features of doubly and singly excited He-like ions receive attention in the study of electron-electron correlation as well as strong relativistic and quantum electrodynamics (QED) effects.

The one-electron one-photon (OEOP) x rays emitted from highly ionized Ni have been experimentally observed in beam foil spectroscopy [12,13], laser-produced and tokamak plasmas [14–17], and electron beam ion trap [18]. On the theoretical side, most of the previous data on OEOP transitions from doubly and singly excited states of He-like Ni are largely based on nonrelativistic or semirelativistic models. The spectra from He- and Li-like Ni have been investigated by Vainshtein and Safronova [19] using the $1/Z$ expansion method. The satellite spectra of He- and Li-like Ni observed by Husan *et al.* [15] from Tokamak Fusion Test Reactor have been interpreted by them using the Hartree-Fock Slater model. Bomarda *et al.* [16] have used SUPERSTRUCTURE code to analyze the He-like to B-like satellite spectra of Ni recorded from Joint European Torus (JET) tokamak. Goryayev *et al.* [20] have carried out modified Z expansion (MZ) calculations with relativistic corrections on the excited states of $2lnl'$ and $1s2lnl'$ ($n = 2$ and 3) configurations. The

relativistic random phase approximation (RRPA) has been applied to study radiative transition from $n = 2$ states along the He-isoelectronic sequence by Lin *et al.* [21]. Vainstein *et al.* [22] have reported $1/Z$ expansion calculations on the energy levels of He- and Li-like ions with the inclusion of relativistic and radiative effects along with parameters for screening and extrapolation by the principal quantum number n. Using mainly Cowan's Hartree Fock model with relativistic corrections (HFR) and also AUTOSTRUCTURE and Multiconfiguration Dirac Fock (MCDF) models to assess the HFR data, Palmeri *et al.* [8] have reported extensive data on the radiative and Auger transitions on the K lines from H-like to C-like nickel. While no experimental work seems to have been carried out on two-electron one-photon (TEOP) transitions in He-like Ni, Safronova *et al.* [23] have reported nonrelativistic data for OEOP and TEOP transitions from He-like Ni using the Coulomb one-electron function. The lifetimes of the less intense electric dipole forbidden transitions ($M1$, $E2$, etc.) have also been shown to be necessary in the interpretation of line intensities and in the analysis of widths and shapes of the spectral line associated with the neighboring allowed transitions [24,25].

In this work, fully relativistic calculations on the various possible radiative transitions from doubly and singly excited He-like Ni with $2p^2$ initial configuration decaying sequentially to $^1S_0$ ground state have been carried out. The energies and rates of the electric dipole allowed and forbidden transitions among the first 15 fine structure levels have been computed in the relativistic configuration interaction formalism (RCI) using MCDF wave functions. To approximate the radial dependence of nuclear charge density, a two-parameter Fermi charge distribution is considered. The electron-electron correlation has been considered in the active space approximation. The purpose of the present study is to provide a complete tabulation of all conceivable electric dipole allowed and forbidden transitions from states of $2p^2$ configuration decaying sequentially to $1s^2$ ground configuration with emphasis on the branching ratios of the various decay channels of doubly and singly excited states. An attempt has been made to analyze the important factors affecting the transition parameters. The

calculations have been carried out using GRASP2K [26], which is a modification of GRASP92 code [27].

II. NUMERICAL PROCEDURE

In a multiconfiguration relativistic calculation, the configuration state functions (CSFs) are symmetry adapted linear combinations of Slater determinants constructed from a set of one-electron Dirac spinors. A linear combination of these configuration state functions (CSFs) is then used in the construction of atomic state functions (ASFs) with the same J and parity.

$$\Psi_i(J^P) = \sum_{\alpha=1}^{n_{\text{CSF}}} c_{i\alpha} \Phi(\Gamma_\alpha J^P),$$ (1)

where $c_{i\alpha}$ are the mixing coefficients for the state i and n_{CSF} are the number of CSFs included in the evaluation of ASF. The Γ_α represents all the one-electron and intermediate quantum numbers needed to define the CSFs and the configuration mixing coefficients are obtained through the diagonalization of the Dirac-Coulomb Hamiltonian,

$$\mathbf{H}_{\text{DC}} = \sum_i \left[c\alpha_i.\mathbf{p}_i + (\beta-1)c^2 - \frac{Z}{\mathbf{r}} \right] + \sum_{i>j} \frac{1}{\mathbf{r}_{ij}}.$$ (2)

Once a set of radial orbitals and the expansion coefficients are optimized for self-consistency, RCI calculations can be performed by including higher order interactions in the Hamiltonian. The most important of these is the transverse photon interaction,

$$\mathbf{H}_{\text{trans}} = \sum_{i,j}^{N} \left[\frac{\alpha_i.\mathbf{p}_i \cos(\omega_{ij})}{\mathbf{r}_{ij}} + (\alpha_i.\nabla_i)(\alpha_j.\nabla_j) \frac{\cos(\omega_{ij})-1}{\omega_{ij}^2 \mathbf{r}_{ij}} \right],$$ (3)

where ω_{ij} is the wave number of the exchanged virtual photon and is obtained as the difference between the diagonal Lagrange multipliers ϵ_i and ϵ_j associated with the orbitals. However, this is valid only when the shells are singly occupied and hence the diagonal energy parameters may not represent the correct binding energies of the orbitals in a variously ionized atomic system. Hence in the present work, the low frequency limit $\omega_{ij} \to 0$ has been adopted and only the mixing coefficients are recalculated by diagonalizing the Dirac-Coulomb-Breit-Hamiltonian matrix. The dominant QED corrections comprise self-energy and vacuum polarization. While the former contribution is evaluated in the hydrogenlike approximation, the later correction is treated perturbatively. The theoretical background necessary for the evaluation of structure parameters is described in detail in the literature [27–30].

The construction of the atomic state functions using systematic expansion of the orbitals in the active space has been discussed in our earlier studies [31]. In this method, the electrons from the occupied orbitals are excited to unoccupied orbitals in the active set. Since the orbitals with the same principal quantum number n have near similar energies, the active set is expanded in layers of n. As the reference configurations corresponding to the different stages of ionization of He-like nickel are different leading to changes in the redistribution of

TABLE I. Excitation energies in cm^{-1} of LSJ states of $2p^2$, $2s2p$, $1s2p$, and $1s2s$ configurations of He-like Ni with respect to $1s^2$ $^1S_0$ ground state. Also listed are the other theoretical level energies and the differences between our energies and the other data sets.

Energy levels		Present	Others	Differences
$1s^2$	$^1S_0$	0	0	0
$1s2s$	$^3S_1$	62356413.98	62359670[a]	−3256.02
			62371255[b]	−14841.02
			62358200[c]	−1786.02
	$^1S_0$	62635238.08	62637030[a]	−1791.92
			62635803[b]	−564.92
			62635400[c]	−161.92
$1s2p$	$^3P_0$	62612817.78	62615790[a]	−2972.22
			62606767[b]	6050.78
			62613700[c]	−882.22
	$^3P_1$	62631592.00	62634560[a]	−2968.00
			62643062[b]	−11470.00
			62634500[c]	−2908.00
	$^3P_2$	62798707.97	62801690[a]	−2982.03
			62810824[b]	−12116.03
			62799900[c]	−1192.03
	$^1P_1$	62953622.93	62956290[a]	−2667.07
			62969714[b]	−16091.07
			62953100[c]	522.93
$2s^2$	$^1S_0$	127109215.32	127111000[a]	−1784.68
$2s2p$	$^3P_0$	127134125.03	127143000[a]	−8874.97
	$^3P_1$	127182190.74	127190000[a]	−7809.26
	$^3P_2$	127357036.82	127362000[a]	−4963.18
	$^1P_1$	127659299.76	127662000[a]	−2700.24
$2p^2$	$^3P_0$	127428756.14	127437000[a]	−8243.86
	$^3P_1$	127547260.20	127554000[a]	−6739.80
	$^3P_2$	127607647.20	127614000[a]	−6352.80
	$^1D_2$	127825041.73	127827000[a]	−1958.27
	$^1S_0$	128115979.27	128117000[a]	−1020.73

[a]Reference [32].
[b]Reference [8].
[c]Reference [19].

electron cloud, to account for a near accurate description of atomic levels, we carried out separate calculations for each set of transitions and generated appropriate wave functions. While the OEOP transitions converged well with the $\{n,l = n\text{-}1\}$ set with $n = 1$ to 4, the TEOP transitions, being correlation sensitive, demanded further expansion of the active space and hence we generated four additional layers of virtual shells with $spdf$ symmetry. To maintain uniformity in numerical computation and to ensure that the most important correlation configurations are captured in the TEOP transitions, the OEOP and TEOP transition parameters were evaluated with the $\{n = 1\text{-}8 \ \ l = 0\text{-}3 \}$ set. The procedure followed in the generation of CSFs was the same for all groups of transitions.

The correlation contribution was evaluated by considering single and double (SD) excitations of electrons from the reference configurations to the orbitals in the active set. We first generated Dirac-Fock wave functions in the Extended Optimal Level (EOL) scheme for the various sets of initial and final configurations. In the EOL method, the radial functions

TABLE II. RCI wavelengths in Å and length gauge rates in s^{-1} for all possible decay modes of $\Delta n = 1$ radiative transitions. The last column lists the ratio of length to velocity gauge rates. The available theoretical and experimental data are also included in the table. The numbers in the parentheses are powers of 10.

Initial state	Final state		Energy Present	Energy Others Theory	Energy Others Expt.	Rate Present	Rate Others	A_l/A_v
$2p^2(^1S_0)$	$1s2p(^3P_1)$	E1(IC)	1.5271	1.5271[a]		3.622(11)	2.64(11)[a]	0.99
	$1s2p(^1P_1)$	E1	1.5346	1.5347[a]	1.5381[b]	6.594(14)	6.95(14)[a]	1.00
	$1s2p(^3P_2)$	M2	1.5310			2.851(10)		
$2p^2(^1D_2)$	$1s2p(^3P_1)$	E1(IC)	1.5339	1.5339[a]		9.312(11)	9.86(11)[a]	0.99
	$1s2p(^3P_1)$	M2	1.5339			2.881(9)		
	$1s2p(^1P_1)$	E1	1.5415	1.5415[a]	1.5417[b] 1.5409[c]	5.225(14)	5.51(14)[a]	1.00
	$1s2p(^1P_1)$	M2	1.5415			7.271(9)		
	$1s2p(^3P_2)$	E1(IC)	1.5378	1.5378[a]		2.161(14)	2.26(14)[a]	1.00
	$1s2p(^3P_2)$	M2	1.5378			2.207(10)		
	$1s2p(^3P_0)$	M2	1.5335			5.075(8)		
$2p^2(^3P_2)$	$1s2p(^3P_1)$	E1	1.5390	1.5390[a]	1.5397[b]	2.443(14)	2.57(14)[a]	1.00
	$1s2p(^3P_1)$	M2	1.5390			7.339(9)		
	$1s2p(^1P_1)$	E1(IC)	1.5467	1.5467[a]		1.589(14)	1.62(14)[a]	1.00
	$1s2p(^1P_1)$	M2	1.5467			2.853(9)		
	$1s2p(^3P_2)$	E1	1.5430	1.5430[a]		3.411(14)	3.55(14)[a]	1.00
	$1s2p(^3P_2)$	M2	1.5430			1.822(9)		
	$1s2p(^3P_0)$	M2	1.5385			6.320(9)		
$2p^2(^3P_1)$	$1s2p(^3P_1)$	E1	1.5405	1.5404[a]		1.645(14)	1.73(14)[a]	1.00
	$1s2p(^3P_1)$	M2	1.5405			1.585(10)		
	$1s2p(^3P_0)$	E1	1.5400	1.5400[a]	1.5409[b]	2.461(14)	2.59(14)[a]	1.00
	$1s2p(^1P_1)$	E1(IC)	1.5481	1.5481[a]		2.102(13)	2.06(13)[a]	1.00
	$1s2p(^1P_1)$	M2	1.5481			1.229(9)		
	$1s2p(^3P_2)$	E1	1.5444	1.5444[a]		3.127(14)	3.21(14)[a]	1.00
	$1s2p(^3P_2)$	M2	1.5444			1.420(5)		
$2p^2(^3P_0)$	$1s2p(^3P_1)$	E1	1.5433	1.5433[a]		6.609(14)	6.87(14)[a]	1.00
	$1s2p(^1P_1)$	E1(IC)	1.5510	1.5510[a]		1.179(13)	1.19(13)[a]	1.00
$2p^2(^3P_0)$	$1s2p(^3P_2)$	M2	1.5473			4.924(9)		
$2s2p(^1P_1)$	$1s2s(^1S_0)$	E1	1.5379	1.5379[a] 1.5374[d]		3.561(14)	3.72(14)[a] 3.71(14)[d]	1.00
	$1s2s(^3S_1)$	E1(IC)	1.5313	1.5314[a]		1.911(13)	2.02(13)[a]	1.00
	$1s2s(^3S_1)$	M2	1.5313			1.500(10)		
	$1s^2(^1S_0)$	E1	0.7834	0.7831[d]		3.875(10)	1.087(11)[d]	1.56
$2s2p(^3P_2)$	$1s2s(^3S_1)$	E1	1.5384	1.5384[a]		3.691(14)	3.88(14)[a]	1.00
	$1s2s(^3S_1)$	M2	1.5384			1.028(10)		
	$1s2s(^1S_0)$	M2	1.5451			6.805(9)		
	$1s^2(^1S_0)$	M2	0.7852			3.048(6)		
$2s2p(^3P_1)$	$1s2s(^1S_0)$	E1(IC)	1.5493	1.5492[a]		2.051(13)	1.97(13)[a]	1.00
	$1s2s(^3S_1)$	E1	1.5426	1.5426[a]		3.537(14)	3.66(14)[a]	1.00
	$1s2s(^3S_1)$	M2	1.5426			2.373(9)		
	$1s^2(^1S_0)$	E1(IC)	0.7863			2.607(9)		1.53
$2s2p(^3P_0)$	$1s2s(^3S_1)$	E1	1.5437	1.5437[a]	1.5430[b]	3.746(14)	3.84(14)[a]	1.00
$1s2p(^1P_1)$	$1s^2(^1S_0)$	E1	1.5885	1.5880[f]	1.5886[b] 1.5887[c] 1.5886[e] 1.5884[h]	6.031(14)	6.06(14)[g]	1.00 1.00
$1s2p(^3P_2)$	$1s^2(^1S_0)$	M2	1.5924		1.5928[c] 1.5922[h] 1.5924[e]	1.194(10)	1.20(10)[g]	
$1s2p(^3P_1)$	$1s^2(^1S_0)$	E1(IC)	1.5967	1.5963[f]	1.5970[c] 1.5969[e]	7.718(13)	7.49(13)[g]	1.00
$1s2s(^3S_1)$	$1s^2(^1S_0)$	M1	1.6037		1.6042[c] 1.6036[e] 1.6034[h]	4.411(8)	4.45(8)[g]	

TABLE II. *(Continued.)*

Initial state	Final state		Energy		Rate		A_l/A_v
			Present	Others Theory Expt.	Present	Others	
$2s^2({}^1S_0)$	$1s2p({}^3P_1)$	$E1(IC)$	1.5509	1.5509[a]	8.746(13)	8.17(13)[a]	1.00
	$1s2p({}^1P_1)$	$E1$	1.5587	1.5587[a]	6.273(13)	6.56(13)[a]	1.00
	$1s2p({}^3P_2)$	$M2$	1.5550		1.186(9)		
	$1s2s({}^3S_1)$	$M1$	1.5443		1.186(9)		

[a]Reference [20].
[b]Reference [16].
[c]Reference [2].
[d]Reference [23].
[e]Reference [15].
[f]Reference [8].
[g]Reference [21].
[h]Reference [17].

and the mixing coefficients are determined by optimizing the energy functional which is the weighted sum of the energy values corresponding to a set of $(2j+1)$ eigenstates. We then generated limited CSFs by allowing SD excitations of electrons from the reference configurations and depending on the initial and final configurations, the number of CSFs from limited correlation varied from four to 15. These optimized CSFs were then used to evaluate the transition parameters of the respective transitions. Then by gradually expanding the size of the active space until the convergence of the observable is obtained, the two sets of SD excitation calculations, one with only correlation and the other with contributions from higher order corrections to the correlated functions were repeated for each step-by-step multiconfiguration expansion taking care of the wave-function convergence criterion (10^{-8}). To ensure numerical stability and to reduce processing time, during each layer by layer expansion of the orbital set arising from incrementing the principal quantum number n by one, only the newly added orbitals were optimized while the previously generated orbitals were kept frozen. In the subsequent RCI calculations, we recalculated the mixing coefficients with a frozen radial set. The ASFs thus generated were transformed

TABLE III. RCI energies in Å and length gauge rates in s^{-1} of $\Delta n = 0$ radiative transitions. Also included in the last column are the ratio of length to velocity gauge rates. The available theoretical rate values are also listed in the table.

Initial state	Final state		Energy	Rate		A_l/A_v
				Present	Others	
$2p^2({}^1S_0)$	$2s2p({}^3P_1)$	$E1(IC)$	107.091	5.504(7)		1.04
	$2s2p({}^1P_1)$	$E1$	218.961	9.548(9)		0.99
$2p^2({}^1D_2)$	$2s2p({}^3P_1)$	$E1(IC)$	155.562	1.961(8)		0.98
	$2s2p({}^1P_1)$	$E1$	603.323	1.435(8)		0.94
	$2s2p({}^3P_2)$	$E1(IC)$	213.689	1.408(9)		0.99
$2p^2({}^3P_2)$	$2s2p({}^3P_1)$	$E1$	235.042	9.848(8)		0.98
	$2s2p({}^3P_2)$	$E1$	399.051	3.289(8)		0.96
$2p^2({}^3P_1)$	$2s2p({}^3P_0)$	$E1$	242.025	1.094(9)		0.98
	$2s2p({}^3P_1)$	$E1$	273.884	5.341(8)		0.98
	$2s2p({}^3P_2)$	$E1$	525.603	1.306(8)		0.94
$2p^2({}^3P_0)$	$2s2p({}^3P_1)$	$E1$	405.530	7.873(8)		0.97
$2s2p({}^1P_1)$	$2p^2({}^3P_0)$	$E1(IC)$	433.854	4.780(7)		0.98
	$2p^2({}^3P_1)$	$E1(IC)$	893.142	8.192(5)		1.21
	$2p^2({}^3P_2)$	$E1(IC)$	1936.956	2.771(6)		1.35
	$2s^2({}^1S_0)$	$E1$	181.560	3.619(9)		0.97
$2s2p({}^3P_1)$	$2s^2({}^1S_0)$	$E1(IC)$	1356.534	1.236(4)		0.14
$1s2p({}^1P_1)$	$1s2s({}^1S_0)$	$E1$	314.510	7.031(8)	7.53(8)[a]	0.99
	$1s2s({}^3S_1)$	$E1(IC)$	167.597	5.810(8)	5.95(8)[a]	1.00
$1s2p({}^3P_2)$	$1s2s({}^3S_1)$	$E1$	226.101	2.096(9)	2.17(9)[a]	0.99
$1s2p({}^3P_1)$	$1s2s({}^3S_1)$	$E1$	363.543	4.411(8)	4.82(8)[a]	0.98
$1s2p({}^3P_0)$	$1s2s({}^3S_1)$	$E1$	390.121	4.007(8)	4.35(8)[a]	0.97

[a]Reference [21].
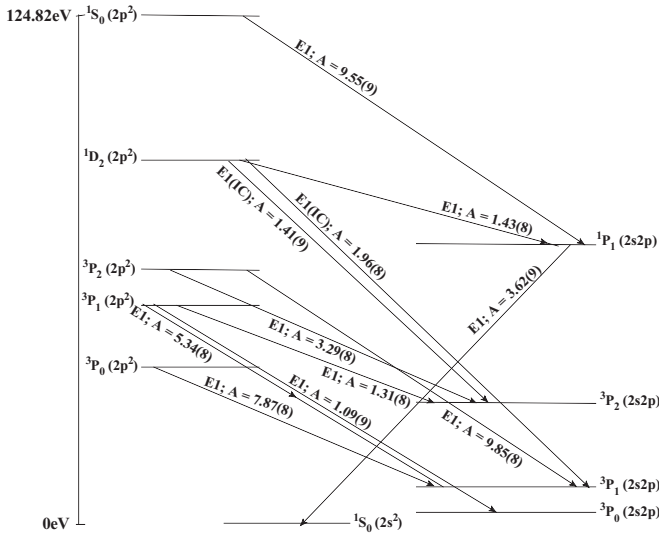
FIG. 1. Partial energy level diagram for $2l2l'$ configurations of He-like Ni. The numbers within the brackets denote powers of ten.

to become bi-orthonormal before computing the transition rates.

III. RESULTS AND DISCUSSION

The calculated excitation energies of the fine structure states of $2p^2, 2s2p, 1s2p, 2s^2$, and $1s2s$ configurations of He-like Ni are listed in Table I. In order to obtain accuracy estimates, the level energies of the various doubly and singly excited states are compared with previous values from the

1/Z expansion [19], Hartree-Fock model with relativistic corrections [8], and the NIST database [32]. While the level energies of singly excited states listed in the NIST database correspond to either the interpolated or extrapolated data obtained from experimental level energies along the isoelectronic sequence, the level energies of doubly excited states are mainly theoretical data with a rough approximation of QED effects. The doubly and singly excited fine structure states lie within the energy ranges of 125–74 eV, respectively, the latter being in accordance with the results reported by Drake [33]. Our level energies compare well with NIST [32] and 1/Z expansion [19] and differ from HFR values [8] by 0.07–2 eV. The small deviations between our values and the other data sets [8,19,32] listed in the last column of the table correspond to the difference in the QED contributions.

Table II lists the energies and length gauge rates of transitions which involve a change of principal quantum number $\Delta n = 1$ for all possible radiative decay modes. The ratios of the length (A_l) to velocity (A_v) gauges rates are given in the last column of the table. We have made a detailed comparison of our results with other theoretical data [8,15–17,20,21,23]. While experimental results for the various fine structure transitions from $1s2p$ configuration are available in literature, to our knowledge, experimental energies on the OEOP transitions from states of $2l2l'$ configuration in He-like Ni are reported only for the intense $2p^2$ ($^1D_2$)-$1s2p$($^1P_1$) transition recorded by Phillips *et al.* [2] in the solar flare spectrum. Using the resonance lines from $2p - 1s$ transitions in H-like Ni as references for calibration, the five satellite peaks observed by Bombarda *et al.* from JET Tokamak [16] were first digitized and then the best fit with Gaussian peaks on the experimental

TABLE IV. The percentage errors in computed transition energies (δE), line strengths (δS), and length form transition rates (δA). The numbers within the brackets denote powers of 10.

Initial state	Final state	δE	δS	δA	Initial state	Final state	δE	δS	δA
$2p^2$	$1s2p$				$2p^2$	$2s2p$			
$^1S_0$	$^3P_1$	$+1.96(-3)$	$-6.82(-1)$	$-1.13(-2)$	$^1D_2$	$^3P_2$	$+6.39(-1)$	-1.52	-1.89
$^1S_0$	$^1P_1$	$+6.52(3)$	$-2.12(-1)$	$-1.51(-2)$	$^1S_0$	$^1P_1$	$+3.74(-1)$	-1.00	-1.11
$^3P_2$	$^3P_1$	$-6.50(-3)$	$-1.68(-1)$	$+2.17(-2)$	$^3P_1$	$^3P_0$	$+5.31(-1)$	-2.08	-1.57
$^3P_2$	$^1P_1$	$-6.47(-3)$	$-1.10(-1)$	$+2.01(-2)$	$^3P_1$	$^3P_1$	$+3.07(-1)$	-2.47	$-9.19(-1)$
$^3P_2$	$^3P_2$	$-6.48(-3)$	$-2.03(-1)$	$+1.61(-2)$	$^3P_0$	$^3P_1$	$-1.66(-1)$	-3.31	$+4.97(-1)$
$^1D_2$	$^3P_1$	$+1.30(-3)$	$-6.79(-1)$	$-1.72(-3)$	$^3P_2$	$^3P_1$	$+3.43(-1)$	-1.88	-1.02
$^1D_2$	$^1P_1$	$+1.95(-3)$	$-1.35(-1)$	$+1.15(-3)$	$2s2p$	$1s2s$			
$^3P_0$	$^3P_1$	$-6.48(-3)$	$-2.08(-1)$	$+9.99(-3)$	$^3P_0$	$^3S_1$	$-6.48(-3)$	$-1.60(-1)$	$+2.64(-2)$
$^3P_0$	$^1P_1$	$-6.45(-3)$	$-2.34(-1)$	$+1.53(-2)$	$^3P_1$	$^3S_1$	$-6.48(-3)$	$-1.56(-1)$	$+1.84(-2)$
$^3P_1$	$^3P_1$	$-6.49(-3)$	$-1.96(-1)$	$+9.72(-3)$	$^3P_2$	$^3S_1$	$+6.50(-4)$	$-1.45(-1)$	$+7.86(-3)$
$^3P_1$	$^3P_0$	$-6.49(-3)$	$-1.88(-1)$	$+2.40(-2)$	$^3P_1$	$^1S_0$	$-1.29(-2)$	$-2.03(-1)$	$+3.07(-2)$
$^3P_1$	$^1P_1$	$-6.46(-3)$	$-2.33(-1)$	$+2.28(-2)$	$^1P_1$	$^1S_0$	$-1.95(-3)$	$-1.67(-1)$	$-2.25(-3)$
$^3P_1$	$^3P_2$	$-6.48(-3)$	$-2.04(-1)$	$+2.49(-2)$	$^1P_1$	$^3S_1$	$+2.61(-3)$	$-9.83(-2)$	$+1.99(-3)$
$^1D_2$	$^3P_2$	$+6.50(-3)$	$-1.90(-1)$	$-1.30(-2)$	$1s2p$	$1s2s$			
$2s^2$	$1s2p$				$^1P_1$	$^1S_0$	$-4.09(-1)$	-1.34	$+1.23$
$^1S_0$	$^3P_1$	$+6.45(-3)$	$-1.12(-1)$	$-1.39(-2)$	$^1P_1$	$^3S_1$	$+8.35(-3)$	$8.16(-2)$	$-2.62(-2)$
$^1S_0$	$^1P_1$	$+1.92(-3)$	$-2.56(-2)$	$+5.90(-3)$	$^3P_2$	$^3S_1$	$+5.88(-2)$	-1.04	$-1.78(-1)$
$2s2p$	$1s^2$				$1s2p$	$1s^2$			
$^1P_1$	$^1S_0$	$-1.28(-2)$	55.69	$+1.47(-2)$	$^3P_1$	$^1S_0$	$-6.26(-3)$	$-3.83(-1)$	$+1.63(-2)$
$^3P_1$	$^1S_0$	$-1.27(-2)$	52.52	$+2.95(-2)$	$^1P_1$	$^1S_0$	$-6.30(-3)$	$-1.87(-1)$	$+2.49(-2)$
$2s2p$	$2s^2$								
$^1P_1$	$^1S_0$	$-3.97(-2)$	-3.15	$+1.16(-1)$					

spectrum using the GFit program [34] was carried out. The experimental spectral lines were identified by comparison of the peak wavelengths and intensities with our RCI predictions on wavelengths and rates. The wavelengths of the experimental peaks of Bombarda *et al.* [16] thus obtained are included in Table II. A comparison shows that our computed wavelengths in general are in good agreement with the digitized data and differ by 0.0002 Å to 0.0009 Å except for the intense $^1S_0$-$^1P_1$ transition. However, our RCI wavelength for $1s2p$ $^1P_1$-$1s^2$ $^1S_0$ transition is in excellent agreement with their resonance line normalized to the their SUPERSTRUCTURE calculations. Though our computed energy for $2p^2(^1D_2)$-$1s2p(^1P_1)$ transition differs from the solar flare observations of Phillips *et al.* [2] by 0.0006 Å, our values for $1s2p$ $(^1P_1, {}^3P_1, {}^3P_2)$-$1s^2$ $(^1S_0)$ transitions are in very good agreement with their data and also with the TFTR plasma measurement of Hsuan *et al.* [15] normalized to their HFS calculations. The present wavelengths are in very good agreement with the TFTR measurements of Bitter *et al.* normalized to $1/Z$ expansion calculations on the resonance line wavelength [17]. The level populations in Tokamak are affected by electron-impact excitation and dielectronic recombination and the difference between our RCI wavelengths and experimental values from tokamak plasmas is mainly due to these effects. Though not included in Table I so as to restrict the length of the table, we notice that our values compare well with the Z expansion data listed in Ref. [17] and also with the HFS values of Husan *et al.* [15] and differ by 0.0004 Å to 0.0013 Å from the SUPERSTRUCTURE results reported by Bombarda *et al.* [16]. However, our energies are in excellent agreement with the relativistic corrections included

MZ calculations of Goryayev *et al.* [20] with a difference of less than 0.0001 Å.

The present OEOP rates for transitions from states of $2l2l'$ and $1s2p$ configurations compare well with the MZ values of Goryayev *et al.* [20] and the relativistic random phase approximation (RRPA) results of Lin *et al.* [21], respectively. The intensities of the spin changing $2p^2(^1D_2)$-$1s2p(^3P_2)$ and $2p^2(^3P_2)$-$1s2p(^1P_1)$ transitions are 40% and 65% of the most intense $E1$ line from the respective initial states. Our calculated $2s2p(^1P_1, {}^3P_1)$-$1s^2(^1S_0)$ TEOP transition energies and rates differ considerably from the nonrelativistic values of Safronova *et al.* [23]. This might be due to the relativistic contraction of the wave functions near the nucleus and the effects of electron-electron correlation. Unlike these weak lines, the anomalous $2s^2(^1S_0)$-$1s2p(^1P_1, {}^3P_1)$ TEOP transitions in which the electrons jump to two different shells compare well with the relativistic MZ data [20]. The intensities of these special types of transitions are just an order of magnitude less than the usual type $E1$ lines from $2p^2$-$1s2p$ transitions. The spin-forbidden line from the $2s^2(^1S_0)$-$1s2p(^3P_1)$ transition is nearly 40% more intense than the allowed $^1S_0$-$^1P_1$ line. This former $E1$ transition is attributed to strong interaction between $2s^2(^1S_0)$ and $2p^2(^1S_0)$ terms and the spin-orbit mixing in the final state. While the energy difference between the $M1$ and $M2$ lines from the respective $2s^2$-$1s2s(^3S_1)$ and $2s^2$-$1s2p(^3P_2)$ transitions is 155 eV, they have the same intensity.

Similar results for transitions which correspond to $\Delta n = 0$ are given in Table III. All the spectral lines from the electric dipole allowed and forbidden transitions lie in the ultraviolet part of the electromagnetic spectrum and are weak
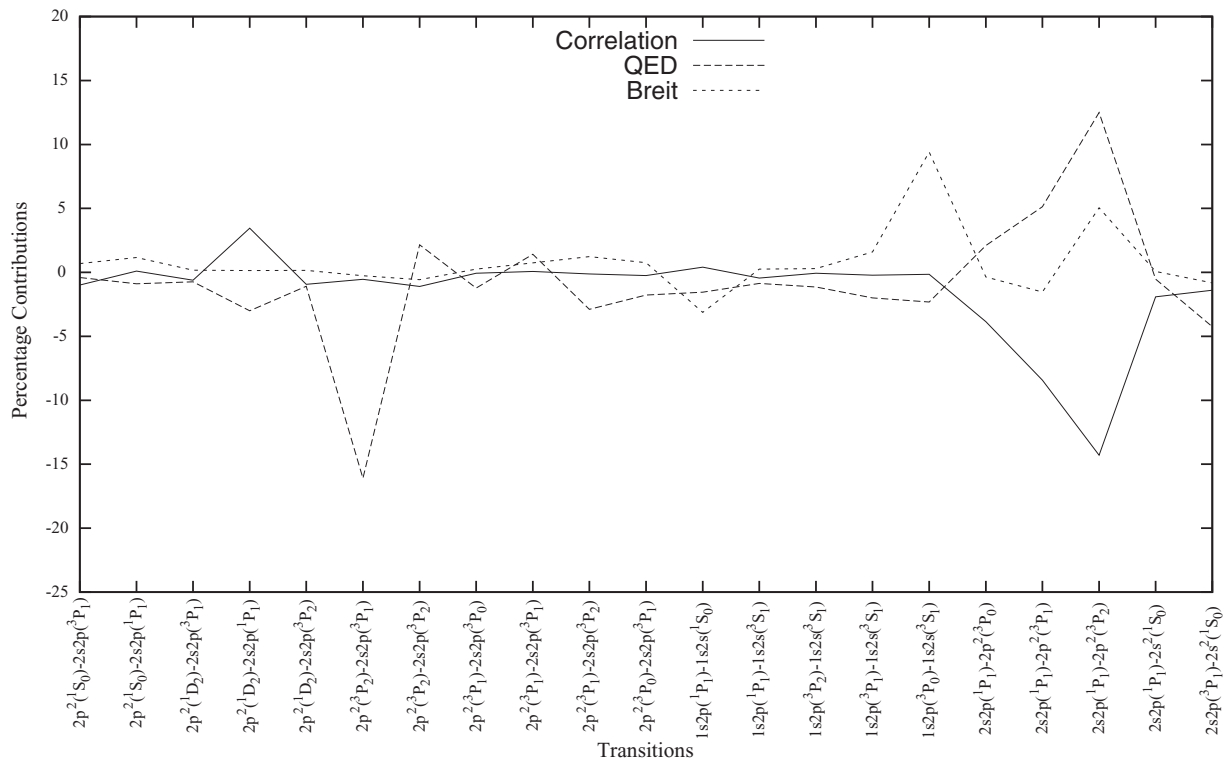
FIG. 2. Correlation energy difference between large and limited configuration state functions to the energies of $\delta n = 0$ transitions. Also shown are contributions from Breit and QED effects.
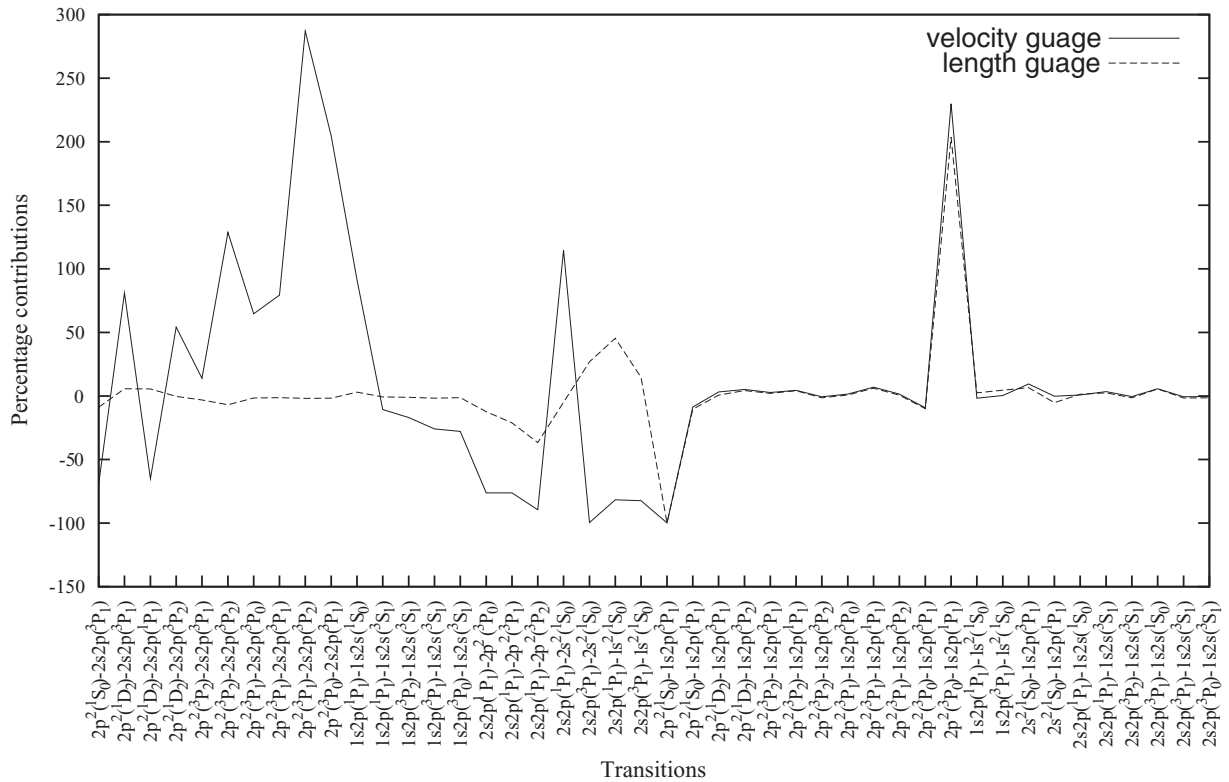
FIG. 3. Correlation contributions to the length (A_l) and velocity (A_v) gauges rates of various transitions from singly and doubly excited states of He-like Ni.

transitions. There seems to be no experimental or theoretical results available for the $\Delta n = 0$ transitions from $2l2l'$ configurations. While experimental values are not available for the various lines from the fine structure states of $1s2s$

and $1s2p$ configurations, RRPA rates are reported by Lin *et al.* [21] for all the transitions. The present rates are in good agreement with the RRPA rates. While the lifetimes of $1s2p$ ($^3P_0$) and $1s2s(^3S_1)$ states are nearly the same, the $E1$ and $M1$
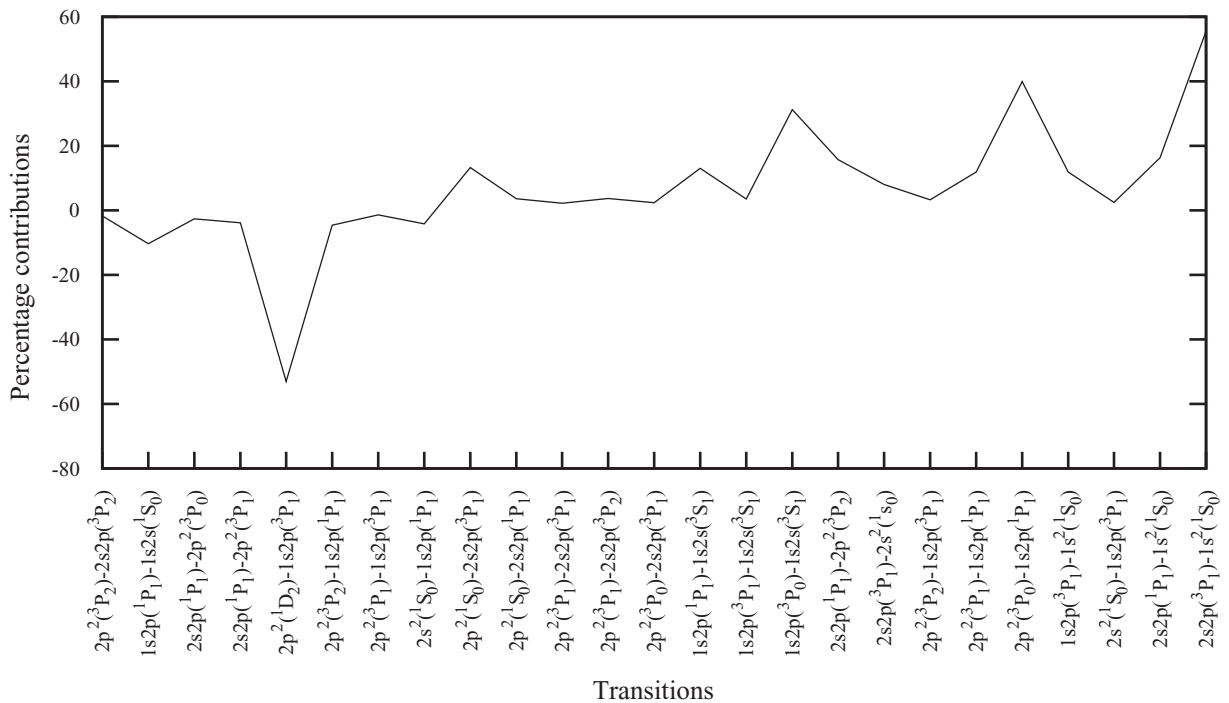
FIG. 4. Breit contributions to the length form (A_l) rates .The legends are the same as in Fig. 3.

transitions from these states are well separated with an energy difference of ~7.7 keV. Following Dunford *et al.* [12], we also observe that the $1s2p(^3P_2)$-$1s^2(^1S_0)$ $M2$ line is stronger than the $E1$ line from $1s2p$ $(^3P_2)$-$1s2s(^3S_1)$. However, our calculations show that except for the above $M2$ transition, the electric dipole forbidden lines from other possible OEOP and TEOP transitions are many orders of magnitude weaker than the $E1$ transitions that dominate most parts of the spectra. Figure 1 shows a partial Grotrian diagram of He-like Ni depicting the nine possible fine structure states of $2p^2$ and $2s2p$ configurations with respect to the $2s^2$ $^1S_0$ state along with their main one-photon decay modes with rates $\geqslant 10^7$ s^{-1}.

It may be mentioned here that while Tables II and III contain all possible $E1$ transitions, to limit the length of the table, we have reported only those forbidden lines with rates greater than $10^4 s^{-1}$. In addition, the extremely weak fine structure transitions among the same configuration are not included in both the tables.

It is seen from Tables II and III that the ratios of the dipole rates in length and velocity forms (A_l/A_v) are unity for most of the transitions and vary marginally for a few transitions. This good agreement between the two results, a necessary condition for accurate wave functions suggest the quality of the radial functions employed in the computation. The strong gauge dependence of the weak TEOP rates might indicate the importance of evaluating both the radial functions and mixing coefficients in the RCI calculations by including full Breit interaction in the self-consistent field calculations [35].

While Table I gives a good agreement between the present level energies and earlier data and A_l/A_v values listed in Tables II and III give an overall indication on the accuracy of our results, we have also tried to critically evaluate the uncertainty in our computed rates. The accuracy of the calculated rates depends both on the line strengths and on the transition energies. In the evaluation of relative errors on transition energies, we have used the NIST level energies listed in Table I as experimental level energies could not be obtained. The uncertainties δS in the length (S_l) and velocity (S_v) forms of line strengths are calculated using the expression $\delta S = (S_l - S_v)/S_v$. With A as the RCI rate and A′ as the rate calculated using the observed transition energies and computed line strengths, the uncertainty with respect to our calculated rate in our computed rate is (δA). The uncertainty estimates δE, δS, and δA are listed in Table IV for some $E1$ transitions from $2l2l'$ and $1s2p$ configurations. It is seen from Table IV that the relative error in the transition energies for all the transitions is within a fraction of a percent and the relative difference in the length and velocity forms of line strengths is well below 0.7% for the $2l2l'$-$1s2l$ transitions. The discrepancy in the line strengths of the intershell transition is slightly larger. Only for the $2s^2$-$1s2p$ transitions, though the deviation in the energies is negligible, the discrepancy in the line strengths is more than 50%.

In Fig. 2, the percentage differences in the $E1$ energies of various transitions evaluated using the set {$n = 1$–8, l} with *spdf* symmetry and the limited CSFs generated from the {$1s2s2p$} reference set are plotted. Also included in this figure are the corrections to the transition energies from Breit interaction and QED effects. Our calculations show that the contributions from these factors to the $\Delta n = 1$ transitions

TABLE V. Branching ratios (BR) and radiative lifetimes (τ) of the initial fine structure levels of He-like Ni. The available theoretical and experimental lifetimes are also included in the table.

Initial state	Final state	BR	τ Present	τ Others Theory	τ Others Expt.
$2p^2(^1S_0)$	$1s2p(^1P_1)$	0.99	1.52 fs		
$2p^2(^1D_2)$	$1s2p(^1P_1)$	0.71	1.35 fs		
	$1s2p(^3P_2)$	0.29			
$2p^2(^3P_2)$	$1s2p(^3P_1)$	0.33	1.34 fs		
	$1s2p(^1P_1)$	0.21			
	$1s2p(^3P_2)$	0.46			
$2p^2(^3P_1)$	$1s2p(^3P_1)$	0.22	1.34 fs		
	$1s2p(^3P_0)$	0.33			
	$1s2p(^1P_1)$	0.03			
	$1s2p(^3P_2)$	0.42			
$2p^2(^3P_0)$	$1s2p(^3P_1)$	0.98	1.49 fs		
	$1s2p(^1P_1)$	0.02			
$2s2p(^1P_1)$	$1s2s(^1S_0)$	0.97	2.66 fs		
	$1s2s(^3S_1)$	0.03			
$2s2p(^3P_2)$	$1s2s(^3S_1)$	1	2.71 fs		
$2s2p(^3P_1)$	$1s2s(^1S_0)$	0.05	2.67 fs		
	$1s2s(^3S_1)$	0.95			
$2s2p(^3P_0)$	$1s2s(^3S_1)$	1	2.67 fs		
$1s2p(^1P_1)$	$1s^2(^1S_0)$	1	1.66 fs	1.65 fs[a] 1.65 fs[b]	
$1s2p(^3P_2)$	$1s^2(^1S_0)$	0.85	71.2 ps	71 ps[a] 70.6 ps[b]	70(3) ps[a] 70(3) ps[c]
	$1s2s(^3S_1)$	0.15			
$1s2p(^3P_1)$	$1s^2(^1S_0)$	1	12.96 fs	13 fs[a] 13.35 fs[b]	
$1s2p(^3P_0)$	$1s2s(^3S_1)$	1	2.50 ns	2.5 ns[a] 2.30 ns[b]	
$1s2s(^3S_1)$	$1s^2(^1S_0)$	1	2.27 ns	2.3 ns[a] 2.25 ns[b]	
$2s^2(^1S_0)$	$1s2p(^3P_1)$	0.58	6.66 fs		
	$1s2p(^1P_1)$	0.42			

[a]Reference [12].
[b]Reference [21].
[c]Reference [13].

are negligible and are appreciable for $\Delta n = 0$ transitions. Hence in the figure, we have considered only the latter type of transitions. It is seen from the figure that the correlation effect decreases the energies of all transitions except $^1S_0 - {}^1P_1, {}^1D_2 - {}^1P_1, {}^3P_1 - {}^3P_1$ transitions from the doubly excited $2p^2$ and $^1P_1 - {}^1S_0$ from singly excited $1s2p$ configurations. Unlike correlation effect, the Breit contribution increases the energies of all transitions except a few transitions. The QED effect decreases the energies of the various fine structure lines except those from $2s2p(^1P_1) - 2p^2(^3P_{0,1,2})$ and $2p^2(^3P_2) - 2s2p(^3P_2)$ transitions.

In Fig. 3, we analyze the influence of correlation on the length and velocity rates of various transitions from singly and doubly excited states of He-like Ni. The correlation contributions from the expanded set were obtained with respect to the limited CSFs set as was discussed earlier. It is seen from Fig. 3 that length gauge rates are not

affected by the expansion of the orbital set except for a few spin forbidden and $2s2p(^1P_1)$-$1s^2(^1S_0)$, $2p^2(^1S_0)$-$1s2p(^3P_1)$, and $2p^2(^3P_0)$-$1s2p(^1P_1)$ transitions whereas velocity gauge rates are largely influenced by the correlation effects and show irregular behavior. It may be mentioned here that it is generally argued that velocity rate is more stable with respect to the changes in the wave functions as contributions to the velocity rates arise mainly from the energy important regions whereas length form rates are influenced by spatial regions unimportant to the energy. However, it is evident from the figure that with limited correlation, the velocity rates are influenced substantially by spurious effects. With significant electron correlation, good convergence between the gauges is obtained except for $2s2p$-$1s^2$ transitions.

We notice from our calculations that the influence of Breit interaction on the length and velocity gauge rates is nearly the same. Hence in Fig. 4, we analyze the effect of Breit interaction only on the length gauge rates of various transitions. It is seen from Fig. 4 that Breit interaction enhances the rates of certain transitions by as much as 40% to 60% and reduces the rates of other transitions by not more than 10% except for the spin changing $1s2p(^3P_1)$-$2p^2(^1D_2)$ transition. For some transitions, there is only a marginal change in the transition rates.

The branching ratios along with the radiative lifetimes of the first 10 doubly excited and five singly excited fine structure levels of He-like Ni are presented in Table V. The lifetimes of the singly excited levels are also compared with the available experimental [12,13] and theoretical [12,21] data. We observe that our calculated values are in excellent agreement with the beam foil [12] and ion atom collision [13] measurements and relativistic predictions [21]. For the $1s2p$ ($^3P_2$) state, the decay to ground state through $M2$ transition is more probable (85%) than the decay to the $1s2s$ $^3S_1$ state through $E1$ transition and hence an experimental measurement on the $M2$ transition would help in studying the sensitivity of relativistic effects on the quadrupole line. It is seen from the table that the lifetimes of the $1s2p$ $^3P_0$ and $1s2s$ $^3S_1$ levels are nearly the same and hence additional information on the lowering of the $^3P_0$ level lifetime due to hyperfine quenching from a fermionic isotope of Ni is needed to differentiate the two levels.

IV. CONCLUSION

In summary, we have investigated the sequential radiative decay of various channels with $\Delta n = 1$ and $\Delta n = 0$ from doubly and singly excited He-like Ni and have analyzed the effects of correlation, Breit, and QED on the transition paremeters. We observe that Breit interaction and QED corrections have quite different effects on different individual transitions. While these effects significantly change the rates of some transitions, for the others, there is a negligible deviation. In general, we find that these higher order corrections are more important for the $\Delta n = 0$ than for the $\Delta n = 1$ transitions of He-like Ni.

While critical compilation on the $\Delta n = 1$ allowed and intercombination electric dipole transitions which belong to $1s^2$, $1s2l$, and $2l2l'$ configurations are available for the ion under consideration, there seems to be no data for $\Delta n = 0$ arising from $2l2l'$. Moreover, data on higher order forbidden transitions with comparable intensity are listed only for one or two transitions. We hope that our newly reported data with uncertainty estimates will help in analyzing the experimental observations.

[1] G. A. Doschek, R. W. Kreplin, and U. Feldman, Astrophys. J. **233**, L157 (1979).

[2] K. J. H. Phillips, Astrophys. J. **605**, 921 (2004).

[3] S. E. Robinson, G. Laughlin, P. Bodenheimer, and D. Fischer, Astrophys. J. **643**, 484 (2006).

[4] K. Koyama *et al.*, Publ. Astron. Soc. Jpn. **59**, S245 (2007).

[5] K. K. Marhas, S. Amari, F. Gyngard, E. Zinner, and R. Gallino, Astrophys. J. **689**, 622 (2008).

[6] T. R. Kallman *et al.*, Astrophys. J. **701**, 865 (2009).

[7] T. Tamura *et al.*, Astrophys. J. **705**, L62 (2009).

[8] P. Palmeri *et al.*, Astrophys. J. **179**, 542 (2008).

[9] A. J. Smith, M. Bitter, H. Hsuan, K. W. Hill, S. vonGoeler, J. Timberlake, P. Beiersdorfer, and A. Osterheld, Phys. Rev. A **47**, 3073 (1993).

[10] C. De Michelis and M. Mattioli, Nucl. Fusion **21**, 677 (1981).

[11] Y. Nakano, S. Suda, A. Hatakeyama, Y. Nakai, K. Komaki, E. Takada, T. Murakami, and T. Azuma, Phys. Rev. A **85**, 020701 (2012).

[12] R. W. Dunford, H. G. Berry, D. A. Church, M. Hass, C. J. Liu, M. L. A. Raphaelian, B. J. Zabransky, L. J. Curtis, and A. E. Livingston, Phys. Rev. A **48**, 2729 (1993).

[13] T. Nandi *et al.*, J. Phys. B **37**, 703 (2004).

[14] B. C. Fawcett, A. Ridgeley, and T. P. Hughes, Mon. Not. R. Astron. Soc. **188**, 365 (1979).

[15] H. Hsuan *et al.*, Phys. Rev. A **35**, 4280 (1987).

[16] F. Bombarda, R. Giannella, E. Kallne, G. J. Tallents, F. Bely-Dubau, P. Faucher, M. Cornille, J. Dubau, and A. H. Gabriel, Phys. Rev. A **37**, 504 (1988).

[17] M. Bitter *et al.*, Phys. Scr. T **37**, 66 (1991).

[18] M. F. Gu, P. Beiersdorfer, G. V. Brown, H. Chen, D. B. Thorn, and S. M. Khan, Astrophys. J. **657**, 1172 (2007).

[19] L. A. Vainshtein and U. I. Safronova, Phys. Scr. **31**, 519 (1985).

[20] F. F. Goryayev, A. M. Urnov, and L. A. Vainshtein, arXiv:physics/0603164.

[21] C. D. Lin, W. R. Johnson, and A. Dalgarno, Phys. Rev. A **15**, 154 (1977).

[22] L. A. Vainshtein and U. I. Safronova, At. Data Nucl. Data Tables **21**, 49 (1978).

[23] U. I. Safronova and V. S. Senashenka, J. Phys. B **10**, L271 (1977).

[24] L. J. Curtis and I. Martinson, Comments At. Mol. Phys. **24**, 213 (1990).

[25] A. Beauchamp, F. Wesemael, P. Bergeron, and J. Liebert, The Astrophy. J. **44**, L85 (1995).

[26] P. Jonsson, X. He, C. Froese Fischer, and I. P. Grant, Comput. Phys. Commun. **177**, 597 (2007).

[27] F. A. Parpia, C. Froese Fischer, and I. P. Grant, Comput. Phys. Commun. **94**, 249 (1996).

[28] I. P. Grant *et al.*, Comput. Phys. Commun. **21**, 207 (1980).

[29] B. J. Mckenzie, I. P. Grant, and P. H. Norrington, Comput. Phys. Commun. **21**, 233 (1980).

[30] I. P. Grant, *Relativistic Quantum Theory of Atoms and Molecules: Theory and Computation* (Springer, New York, 2007).

[31] L. Natarajan, J. Phys. B **35**, 3179 (2002).

[32] Online bibliographic database at NIST, http://physics. nist.gov/asd3.

[33] G. W. F. Drake, Can. J. Phys. **66**, 586 (1988).

[34] A. Kramida (private communication).

[35] R. Kadrekar and L. Natarajan, Phys. Rev. A **84**, 062506 (2011).